ORIGINAL PAPER

The prediction of the coefficient of restitution between impacting spheres and finite thickness plates undergoing elastoplastic deformations and wave propagation

Itzhak Green

Abstract The coefficient of restitution (COR) is a pragmatic analytical tool needed to solve impact problems. The coefficient is customarily obtained empirically by executing experiments intended to mimic actual collision situations. The coefficient depends on many parameters, some of which are the colliding bodies' structures, their material properties, the impact velocities, friction and spin, surface roughness, contamination, and in some cases even adhesion. A comprehensive model that encompasses all parameters is understandably elusive, but if the problem is limited to co-linear impact between two smooth elastic or elastoplastic bodies, particularly two spheres or a sphere and a plate, then a few analytical models are available to predict the COR. A recent model (Jackson et al. in Nonlinear Dyn 60:217–229, 2010) has specifically targeted the elastoplastic deformation caused by the collision while excluding other effects. Other models (notably by Zener (Phys Rev 59(8):669–673, 1941)) do not consider the elastoplastic deformation, focusing only the ensuing elastic waves instigated in a perfectly elastic collision. The said two models may rest at the outermost ends of the effects that influence the apparent coefficient of restitution. The subject of this work is to investigate the interplay of these two models and fuse them into a single model that include both effects of elastic waves in the presence of elastoplastic deformation and vice versa. Then, the new model is compared to recent experimental results by Higgs, et al. (2013, 2018) as well as their FEA simulations (2017). It is shown that a straightforward use of the new model herein predicts quite accurately the apparent coefficient of restitution, where a very good agreement is found between the predictions and the results obtained from experiments and FEA simulations. The comparison is performed for a wide variation of material property combinations, plate thickness-to-sphere diameter ratios, and impact speeds.

Abbreviations

C Poisson's ratio coefficient, Eq. (2)
E Elastic modulus
d Sphere diameter
e Coefficient of restitution
F Contact force according to Zener
h Half plate thickness
k Proportionality coefficient between F and s
m Mass
P Contact force
R Radius
r Sphere radius (Zener's notation), $d/2$
S_y Yield strength

I. Green (✉)
School of Mechanical Engineering, Georgia Institute of Technology, 30332-0405 Atlanta, Georgia
e-mail: itzhak.green@me.gatech.edu

s	Relative displacement (interference), z-U
T	Time parameter according to Zener
t	Plate thickness, $2h$
V	Velocities at initiation and end of contact
U	Surface displacement
v	Velocity
z	Absolute degree of freedom
ε_y	Yield strength-to-elastic modulus ratio, Eq. (3)
λ	Zener's "inelasticity" parameter
v	Poisson's ratio
ρ	Density
σ	Nondimensional relative displacement, Eq. (9)
τ	Nondimensional time, Eq. (9)
ω	Interference between sphere and surface

Subscripts

0	When $s = 0$ (and $\sigma = 0$)
1	Value before impact
2	Value after impact
a	Sphere
b	Plate
c	Critical value
e	Elastic regime
ep	Elastoplastic regime
o	Impact velocity according to Zener
y	Yield
ze	According to Zener

Superscripts

'	Equivalent, Eq. (1)
*	Normalized by a critical value

1 Introduction

The coefficient of restitution (COR) is a necessary ad hoc concept, which once interjected, provides the missing information (i.e., an equation) to complement the conservation of momentum and readily solve impact problems. The utility of the COR is vast in solving problems of engineering, science, sports, and recreation. In its most basic form the COR is a ratio between two impulses: the restitution impulse and the deformation impulse [1]. Upon using the equivalence between impulse and momentum, the COR emerges also as the ratio between the relative velocity of separation after impact and the relative velocity of approach before impact.

The difficulty, however, is that the COR is a parameter that needs to be obtained or estimated somehow. The customary way to determine the COR is by running experiments that mimic actual conditions of the collision and then to offer empirical COR values. Of course, this process is laborious, but in many cases, it is necessary. Under some constraints, the alternative is to estimate the CORs from models that are available. At the conditions of co-linear collision of spheres against each other or of a sphere against a flat surface, various models have been offered over the years. This study specifically focusses on five works. The historic work by Zener [2] offers an analytical solution for the COR of an elastic sphere pinging a thin elastic plate. This model is briefly summarized herein; however, some clarifications are made to qualify some of Zener's definitions. Most notably, his estimation of the COR is dependent upon the ratio of the sphere's diameter to the thickness of the plate (among other parameters). That COR estimation appears to fit reasonably well with the experimental results and analysis offered by Raman [3]. Tsai et al. [4] recast Zener's work to offer an approximate solution for the force–time collision curve between the sphere and plate as a function of Zener's "inelasticity" parameter; however, the issue of the COR is not addressed. There are other recent publications on impact calculations including wave propagation in both colliding bodies [5–8]. These usually require expensive computational effort and they are alternative approaches to the classical approach taken here.

The works by Jackson et al. [9] and Higgs et al. [10–12] have each detailed substantial literature coverages, along with the extensive literature review on impact problems and COR models by Banerjee et al. [13]. These are quite recent and relevant. A massive literature coverage is therefore redundant and is not repeated. Herein, just the utmost relevant models are recast and summarized while adding important new insights. This work provides a simple yet accurate empirical expression to calculate Zener's COR. The JGM model by Jackson et al. [9] is recast, and fused together with Zener's model to provide one effective model for the calculation of the COR which accounts for both elastoplastic deformations and wave propagation for any plate thickness-to-sphere diameter ratio. The new model is compared against recent experimental and FEA simulation results offered by Higgs

et al. [10–12], and conclusions regarding its effectiveness, accuracy, and utility are drawn. Lastly, the interplay of the various parameters that comprise the new model are investigated and discussed.

2 The elastoplastic JGM model

The model developed by Jackson et al. [9] to calculate the COR is one of the two corner stones in this study, and it is now summarized. Based on the JG model [14] to calculate the elastoplastic deformation between a sphere and a half-space flat, reference [9] offers empirical equations for the COR. The deformation phase is based upon [14], where two options are offered for the calculation of the restitution phase according to [15] and [16]. Starting with the equivalent elastic moduli of the contacting bodies (see also definitions in the nomenclature):

$$E' = \frac{E_a' E_b'}{E_a' + E_b'} \quad @ \quad E_i' = \frac{E_i}{1 - v_i^2} \quad i = a, b \quad (1)$$

In this work, in most cases, at least one of the contacting materials is ductile. When both bodies are ductile and also have different material properties, particularly if the yield strengths, S_{ya}, and, S_{yb}, are dissimilar, then it is *imperative* to use the procedure detailed by Green [17] to calculate the forthcoming critical parameters (significant errors will ensue otherwise). Briefly, in normal elastic contacts, Green [17] defined the ratio between the maximum contact pressure, p_o, and the maximum von Mises stress, $\sigma_{e\text{-}max}$, to be $C = p_o/\sigma_{e\text{-}max}$, a ratio found to solely dependent upon the Poisson ratio. A rather accurate curve-fit to a numerical solution of a transcendental equation renders for 3D contacts, $C(v) = 1.295 \, exp(0.736v)$. Abiding by the von Mises yielding criterion, $\sigma_{e\text{-}max} = S_y$ at yielding onset, such that the product $C(v) \cdot S_y$ gives the corresponding critical contact pressure, $(p_o)_c \equiv CS_y$, for each material. For dissimilar materials (as are many of the cases investigated herein), Green [17] teaches that the smallest between these two possibilities decides which of the contacting bodies yields first. Hence:

$$CS_y = \min[C(v_a)S_{ya}, C(v_b)S_{yb}] \quad @ \\ C(v) = 1.295 \exp(0.736v) \quad (2)$$

The equivalent strain at yielding, ε_y, is needed in the upcoming COR expressions. It follows the same logic as above, complementing Eq. (2):

$$\varepsilon_y = \frac{S_{ya}}{E'} \quad \leftrightarrow \quad C(v_a)S_{ya} \leq C(v_b)S_{yb} \\ \varepsilon_y = \frac{S_{yb}}{E'} \quad \leftrightarrow \quad C(v_a)S_{ya} > C(v_b)S_{yb} \quad (3)$$

The critical interference, ω_c, and the critical load, P_c, are also derive in [17]:

$$\omega_c = \left(\frac{\pi \cdot CS_y}{2E'}\right)^2 R \quad (4)$$

$$P_c = \frac{4}{3}\left(\frac{R}{E'}\right)^2 \left(\frac{\pi}{2} CS_y\right)^3 \quad (5)$$

where R is the composite radius calculated according to $1/R = 1/R_a + 1/R_b$. For the current case, the plate's radius $R_b \to \infty$, so $R \equiv R_a$ is the sphere's radius. The critical velocity is derived in [9] by equating the critical strain energy stored (as derived in [17]), $U_c = (\pi \cdot CS_y)^5 R^3/(60E'^4)$, with the impacting sphere kinetic energy at yielding onset, $m_a V_c^2/2$. After simplifications, along with Eqs. (4) and (5), we have:

$$V_c = \sqrt{\frac{4\omega_c P_c}{5m_a}} \quad (6)$$

Specifically, V_c is the initial impact velocity of m_a causing the onset of yielding (in the sphere and/or the plate), causing a critical interference, ω_c, and producing a critical contact force, P_c. Any impact velocity, V_1, that is smaller than V_c would not cause plastic deformation for which, by definition, the $COR = 1$. Defining a normalized impact velocity, $V_1^* = V_1/V_c$, and skipping all the details in [9], only the bottom-line results are of interest here. So, for $0 < (V_1)^* < 1$, the COR is $e = 1$. Note that because reference [9] permits two restitution phase models [15] and [16], two expressions are conceived for the predicted COR at circumstances of elastoplastic impacts. The first model is:

$$e_{44} = 1 - 0.1\ln(V_1^*)\left(\frac{V_1^* - 1}{59}\right)^{0.156} \quad \leftrightarrow \quad 1 < V_1^* \leq 60 \\ e_{44} = 1 - 0.1\ln(60) - 0.11\ln\left(\frac{V_1^*}{60}\right)(V_1^* - 60)^{2.36\varepsilon_y} \leftrightarrow \quad 60 < V_1^* \leq 1000 \quad (7)$$

The subscript 44 is appended to collectively signify that these expressions appear in Eqs. (43) and (44) of Ref. [9], and are given piecewise for two nondimensional velocity ranges. The second model is given by a single equation for the entire nondimensional velocity range:

$$e_{45} = 1 - 0.0361\left(\varepsilon_y\right)^{-0.114}\ln\left(V_1^*\right)\left(V_1^* - 1\right)^{9.5\varepsilon_y}$$
$$\leftrightarrow \quad 1 < V_1^* \leq 1000 \tag{8}$$

Again, the subscript 45 signifies that this is Eq. (45) in Ref. [9]. As Ref. [9] builds upon Ref. [14] it inherits its assumptions. Namely, that impact occurs between a sphere and a half-space. So clearly, this model and these equations are impervious to the thickness of a "plate." Practically, though, these expressions may be applied for spheres impacting "finite thickness" plates when the plate thickness-to-sphere diameter ratio is above a finite value, (which is not necessarily "very large," as shall be seen herein). In the following, either Eq. (7) or (8) will be referred to generically as e_{ep}.

3 The zener model

The model developed by Zener [2] to calculate a COR is the second corner stone of this work. It deals with the conditions that Ref. [9] does not consider. According to Zener's model, the COR is the outcome of an elastic wave instigated in a plate by an impacting sphere. On the wave rebound, the plate ejects the sphere from its surface after some elapsed time from the instant of impact. As was done in the previous section, a summary of Zener's model is recast with a few new observations that are necessary. For consistency and clarity in this section, Zener's original nomenclature for variables is adhered to. Explicitly, t is time, and $2h$ is the plate thickness.

Zener solves the acoustics problem by starting off with the equation of motion (EOM) for an elastic thin plate being pinged by an elastic sphere. The second EOM is that of the sphere, and both EOMs are then coupled by a purely elastic Hertzian contact force acting between sphere and plate. On the rebound, separation occurs when the Hertzian force returns to zero. That force is proportional to the relative coordinate, $s = z{-}U$, i.e., between the sphere degree of freedom, z, and the plate displacement of its surface at the point of contact $U(x = 0, y = 0, t)$. Thus, s signifies the interference. Conveniently, Zener defines dimensionless variables that allow the immediate interpretation of the solution. These are:

$$s = Tv_0\sigma ; \quad t = T\tau \tag{9}$$

where T is a constant with the dimensions of time, and v_0 (using Zener's notation) is the sphere impacting velocity. He found that $T = (m/kv_0^{1/2})^{2/5}$, where m is the sphere mass, and k is the proportionality coefficient between the force, F, and the interference, s, in a Hertzian nonlinear relationship, $F(s) = ks^{3/2}$, such that $k = (4/3)r^{1/2}E'$ (while, k is constant, it ought not be regarded as a "linear spring stiffness"—see the Appendix for additional discussion). An ordinary differential equation (ODE) is developed for the nondimensional relative coordinate between sphere and plate, σ, where τ is a nondimensional time [2]. The nonlinear ODE is:

$$\frac{d^2\sigma}{d\tau^2} + \left(1 + \lambda\frac{d}{d\tau}\right)\sigma^{\frac{3}{2}} = 0 \tag{10}$$

An expanded form of which is given in the Appendix. The equation is subject to the initial conditions:

$$\left.\begin{array}{c} \sigma = 0 \\ \frac{d\sigma}{d\tau} = 1 \end{array}\right\} \ at \ \tau = 0 \tag{11}$$

The nondimensional parameter, λ, in Eq. (10) is identified by Zener as the "*inelasticity parameter*," and it is given by:

$$\lambda = \frac{\pi^{\frac{3}{5}}}{\sqrt{3}}\left(\frac{d/2}{2h}\right)^2\left(\frac{v_0}{v'}\right)^{\frac{1}{5}}\left(\frac{\rho_a}{\rho_b}\right)^{\frac{3}{5}}\left(\frac{E_a'}{E_a' + E_b'}\right)^{\frac{2}{5}} \tag{12}$$

The impacting sphere velocity, v_o, is normalized by the speed of sound in the solid plate:

$$v' = \sqrt{\frac{E_b'}{\rho_b}}$$

Being a nonlinear equation, Zener integrated Eq. (10) numerically with λ as a parameter. Figure 1 shows the numerical solution for three values of the parameter, $\lambda = \{0, 0.75, 1.5\}$. It should be noted that the ordinate in Fig. 1 is proportional to the contact force because via Eq. (9), $F(\sigma) = k(Tv_0)^{3/2}\sigma^{3/2}$. Clearly upon the rebound, when $\sigma = 0$ also $F(\sigma) = 0$, i.e.,

Fig. 1 Numerical solutions of Eq. (10) for three values of λ, and the solution of linearized Eq. (14) for $\lambda = 0$ (the solid lines are for the normalized relative coordinate, $\sigma(\tau)$; the dashed lines are for the normalized negative relative velocity, $-\sigma'(\tau)$)
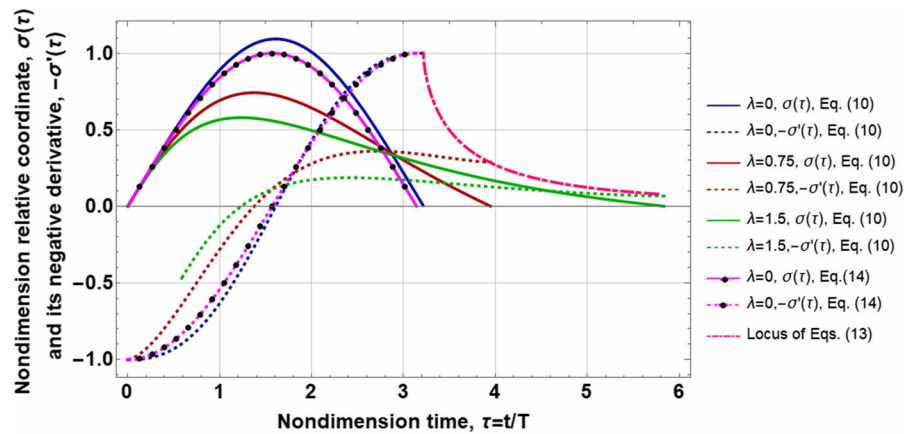
contact is undone, signifying the onset of separation. As indicated by Zener, the COR is the value of $\sigma' = d\sigma/d\tau$ upon the return of σ to zero. However, since σ is defined in the same direction of the sphere initial velocity, v_o, a correction is needed: the COR must be the value of $-\sigma'$ upon σ returning to zero.

Unfortunately, solutions for Eq. (10) are given in [2] for only four values of λ. Hence, that equation is integrated herein numerically for a very dense set of λ (of over 500 values), in the range $0 \leq \lambda \leq 1.5$. At the instant when σ returns to zero, the value of $-\sigma'$ is recorded as the COR for that value of λ. An exponential fit is then applied to that numerical data, giving,

$$e_{ze} = \exp(-1.68374\lambda) \tag{13}$$

The Appendix discusses Eq. (13) further and shows plots of the fit along with the numerical data. The fit mean error is a mere 0.5% with a standard deviation of 0.35%. Equation (13) is a robust analytical representation of Zener's COR as a function of λ.

To complement the analysis, also the total normalized elapsed time, τ_0, is recorded during the process above. So τ_0 represents the nondimensional time at the instant when σ returns to zero on the rebound, i.e., it is the total nondimensional time that the sphere and plate are in compressive contact. That time is also fit as a function of λ with similar accuracy as above, but it is found to essentially increase exponentially with $\lambda^{3/2}$ according to:

$$\tau_0 = 3.215 \exp(0.318\lambda^{\frac{3}{2}}) \tag{13a}$$

Equation (13) and (13a) are both functions of the parameter, λ, the locus of which is also shown in

Fig. 1, effectively representing Zener's COR as a function of τ_0. The locus curve (i.e., the COR) can also be obtained by eliminating λ between the said equations to yield:

$$e_{ze} = \exp\left[-3.61402(\ln \tau_0 - 1.16783)^{\frac{2}{3}}\right]$$
$$@ \ \tau_0 \geq 3.215 \tag{13b}$$

where according to Eq. 13a, for $\lambda = 0$, the smallest nondimensional contact time is $\tau_0 = 3.215$. See the additional discussion in the Appendix.

The analysis presented by Zener is not free of assumptions. First, it is assumed that the plate is wide enough so that reflected waves from the boundaries would not affect the ejection of the sphere. Secondly, it is important to note that the "*inelasticity parameter*," λ, as identified by Zener [2] (and so referenced repeatedly by others) has nothing to do with *inelasticity*. All of the variables in its definition (see Eq. (12)) are unrelated to yielding, plasticity, or permanent set. To the contrary, the parameter λ contains *elasticity* parameters. The consequence is that upon impact completion, i.e., after the sphere is ejected from the plate, their surfaces remain unblemished (regardless of Zener's COR value). Actually, the COR predicted by this theory is the result caused by the plate surface to *elastically* rebound, and after the passage of a time delay, τ_0, eject the sphere at either the same speed (if $\lambda = 0$), or a reduced speed (if $\lambda > 0$) compared to the initial condition (i.e., impacting speed). This is similar to the action of a trampoline.

Further examination of the parameter λ, as given by Eq. (12), is when $d/(2h) \rightarrow 0$ (i.e., when the plate thickness approaches a half-space), then $\lambda \rightarrow 0$, and

the $COR \rightarrow 1$, indicating a perfectly "*elastic*" impact. Observing in Fig. 1 the nonlinear solution for σ when $\lambda = 0$, it seems that the plate surface and the sphere undergo a motion that exhibits a nearly classical half harmonic cycle. So, this condition is examined further. Letting $\lambda = 0$ in Eq. (10) removes one of the nonlinearities. Noting also in Fig. 1 that the nonlinear solution for $max(\sigma)$ is about one unit, so linearizing the power of *(3/2)* (originating with the Hertzian model) would have a somewhat lessened effect. Hence, for $\lambda = 0$, and upon linearization of the power, Eq. (10) simplifies to:

$$\frac{d^2\sigma}{d\tau^2} + \sigma = 0 \qquad (14)$$

having the same initial conditions as given by Eq. (11). The numerical solution of Eq. (14) is also shown in Fig. 1 (by the only lines spotted with the dotted symbols); noting that indeed the linear and nonlinear solutions for σ are close, the velocities, σ', seem even closer, and most importantly, $\sigma' = 1$ in both cases upon the return of σ to $\sigma = 0$. That is, both Eqs. (10) and (14), nonlinear and linear, respectively, result in the *identical COR = 1*. A mechanical equivalent that is governed by Eq. (14) is easily envisioned, and it is shown in Fig. 2, where m_b represents an equivalent plate inertia (the plate elasticity may be conferred to a spring stiffness, if desired). The Appendix offers additional useful discussions. That mechanical equivalent is serving us next.

4 The fusion of JGM's and Zener's models

Consider the mechanical equivalent model in Fig. 2. Suppose first that the only COR existing between sphere, *a,* and plate, *b,* is the result of an elastoplastic impact as obtained by JGM [9]. That COR is
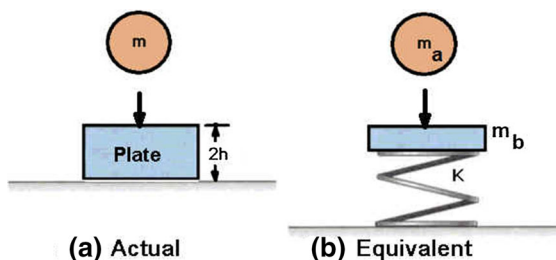
Fig. 2 Actual and equivalent systems

designated by e_{ep}. Initially, before impact, m_a has a velocity v_{a1}, while mass m_b is stationary, i.e., $v_{b1} = 0$. Immediately following impact, mass m_b is disturbed to gain a velocity v_{b2}, while mass m_a acquires a new velocity v_{a2}. Velocities are defined positive in the direction of v_{a1}. In the absence of any external forces, linear momentum is conserved before and after impact:

$$m_a v_{a1} + m_b v_{b1} = m_a v_{a2} + m_b v_{b2} \qquad (15)$$

The classical definition of the COR is:

$$e_{ep} = \frac{v_{b2} - v_{a2}}{v_{a1} - v_{b1}} \qquad (16)$$

Solving these two equations simultaneously for the unknown velocities after impact gives:

$$v_{a2} = \frac{(m_a - e_{ep}m_b)v_{a1}}{m_a + m_b}$$
$$v_{b2} = \frac{(1 + e_{ep})m_a v_{a1}}{m_a + m_b} \qquad (17)$$

Suppose a diagnostics system (e.g., a high speed camera such as in [10, 12]) is focused solely on m_a and thus reporting measured data only on its two velocities, v_{a1} and v_{a2}. Using v_{a2} from Eq. (17), the *apparent* COR resulting from the said measurements is (without a subscript):

$$e = -\frac{v_{a2}}{v_{a1}} = \frac{e_{ep} - \frac{m_a}{m_b}}{1 + \frac{m_a}{m_b}} \qquad (18)$$

Equation (18) is consistent also with Zener's COR definition because it is similarly based on two observations of the sphere's velocities before and after impact (see the discussions following Eq. (14) in Ref. [2], and Eq. (12) herein). Zener's analysis, however, pertains to perfectly elastic conditions between the sphere and the plate, i.e., $e_{ep} = 1$. While, the mass of the sphere, m_a, is obvious, the effective plate mass, m_b, is now determined by allowing e mimic Zener's COR, e_{ze}. Hence, solving Eq. (18) under the conditions, $e_{ep} = 1$, and $e \equiv e_{ze}$, results in:

$$m_b = \frac{(1 + e_{ze})m_a}{1 - e_{ze}} \qquad (19)$$

Substituting Eq. (19) back into Eq. (18) produces the ultimate *apparent* COR,

$$e = \frac{1}{2}\left(e_{ep} + e_{ze} + e_{ep}e_{ze} - 1\right) \qquad (20)$$

This equation encompasses two effects: the outcome of the elastoplastic deformations and the elastic waves. Equation (20) provides the *apparent* COR based on only two observations, i.e., the two velocities v_{a1} and v_{a2}, which are reported by a diagnostics system. This equation is entirely analytical and simple to employ. Both CORs, e_{ep}, and, e_{ze}, are of equal weight. It is easily verified that at the limiting case when there is no elastoplastic damage, say, an impact between two perfectly brittle materials, where $e_{ep} = 1$, Eq. (20) results in $e = e_{ze}$, as expected. That result will pan out later, and seen in Fig. 3d.

The other limiting case, is when the plate is a half-space where according to Eqs. (12) and (13), respectively, $\lambda \rightarrow 0$, and, thus, $e_{ze} \rightarrow 1$, leading Eq. (20) to

approach $e \rightarrow e_{ep}$. To accentuate this point, when $e_{ze} \rightarrow 1$, $m_b \rightarrow \infty$ (see Eq. (19)), causing $v_{b2} \rightarrow 0$ see Eq. (17)), i.e., m_b that was stationary before impact, remains so after impact, as expected from an "infinitely heavy" inertia of the half-space. Then, indeed, all CORs in Eqs. (16), (18), and (20) converge to the same, $e \equiv e_{ep}$. That infers that the only effective COR, is that caused by the elastoplastic deformation, which is where this section IV starts. Practically, though, it will be seen in the following from the experimental and FEA results, as well as from Eq. (20), that e approaches asymptotically e_{ep} even for plates of finite thickness with ratios of thickness to sphere diameter in the order one unit (i.e., such plates depart
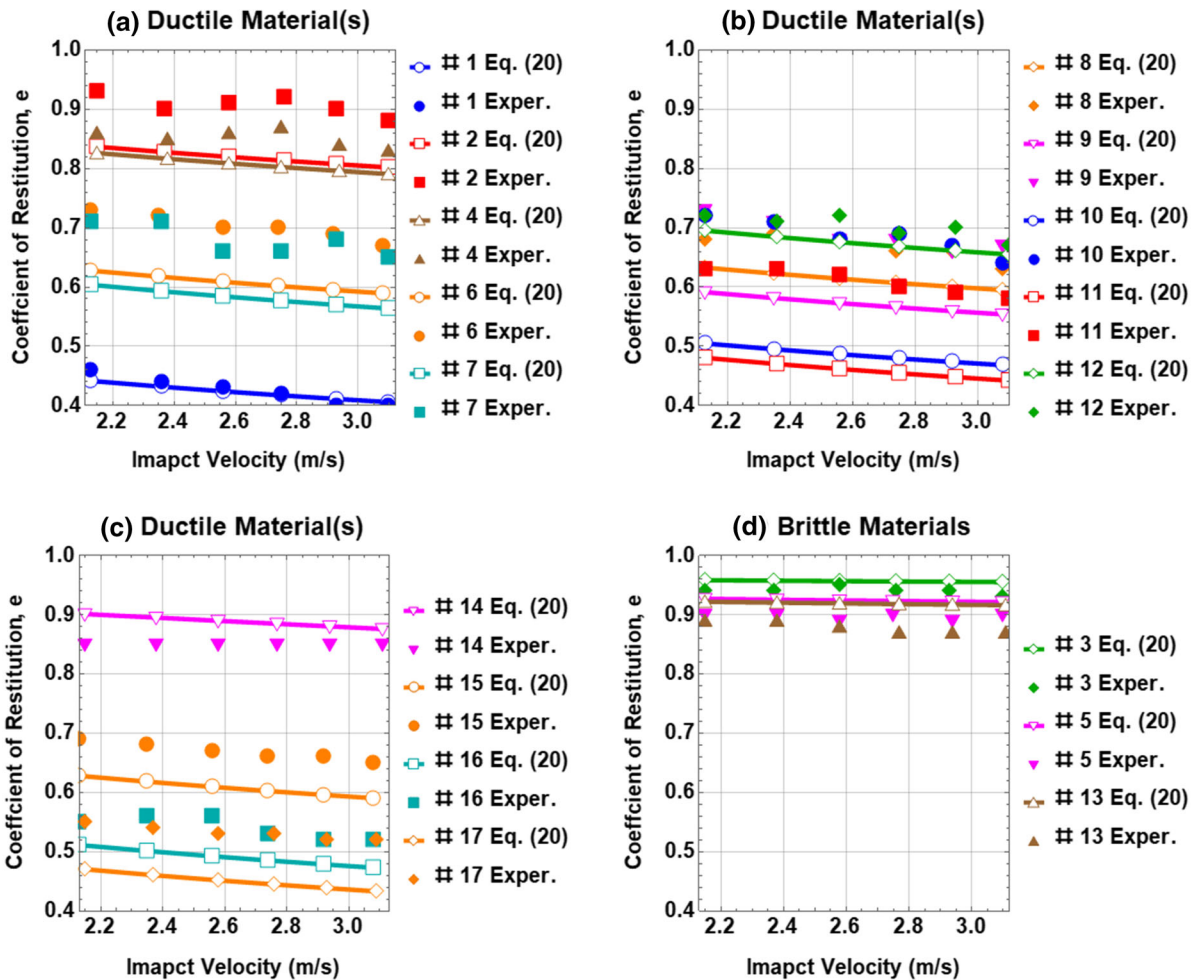

Fig. 3 Comparison between experimentally obtained CORs in Ref. [10] and those calculated herein by Eq. (20). Case numbers (#) are consistent with the list in Table 1. In subfigures (a)-(c) at least one of the materials is ductile. In subfigure (d) both materials are brittle

Table 1 Material properties for the spheres used in the experiments of [10] and target plates (see also Table 2)

No.	Sphere material	Yield strength S_y (Pa)	Sphere diameter d_s (m)	Density ρ (kg/m³)	Poisson's ratio ν	Plate material
1	Aluminum, 110-H16[a]	1.03E + 08	0.00635	2710	0.33	S7 Tool Steel
2	Borosilicate glass[b]	1.00E + 12*	0.00476	2214	0.30	S7 Tool Steel
3$	Borosilicate glass[b]	1.00E + 12*	0.00476	2214	0.30	Borosilicate glass
4	Borosilicate glass[b]	1.00E + 12*	0.00635	2214	0.30	S7 Tool Steel
5$	Borosilicate glass[b]	1.00E + 12*	0.00635	2214	0.30	Borosilicate glass
6	Brass, alloy 260[b]	3.93E + 08	0.00476	8525	0.35	S7 Tool Steel
7	Brass, alloy 260[b]	3.93E + 08	0.00635	8525	0.35	S7 Tool Steel
8	Chrome Steel[a]	1.38E + 09	0.00476	7700	0.30	S7 Tool Steel
9	Chrome Steel[a]	1.38E + 09	0.00476	7700	0.30	Stainless Steel
10	Low Carbon Steel[b]	3.03E + 08	0.00476	7833	0.30	S7 Tool Steel
11	Low Carbon Steel[b]	3.03E + 08	0.00635	7833	0.30	S7 Tool Steel
12	NiTiNOL 60[c]	1.00E + 12*	0.00635	6700	0.34	S7 Tool Steel
13$	NiTiNOL 60[c]	1.00E + 12*	0.00635	6700	0.34	NiTiNOL 60
14	S2 Tool Steel[b]	2.00E + 09	0.00635	7861	0.30	NiTiNOL 60
15	S2 Tool Steel[b]	2.00E + 09	0.00476	7861	0.30	S7 Tool Steel
16	Tungsten Carbide[a]	1.72E + 09	0.00476	14,950	0.18	S7 Tool Steel
17	Tungsten Carbide[a]	1.72E + 09	0.00476	14,950	0.18	Stainless Steel

[a]Small Parts,Inc., [b]McMaster-Carr, [c]NASA Glenn Research Center, [d]Precision Associates, Inc., $Brittle materials for both sphere and plate, *For all brittle materials, the "yield strengths" are pretended to have a very large value of 10^{12} Pa to ward off "yielding" in calculations

considerably from the definition of a "half-space"). That will be seen later in Fig. 6.

It is also important to qualify the limits and conditions under which Eq. (20) may render unusual results. First, note that Zener's range for λ is {0, 1.5}. The upper limit, $\lambda = 1.5$, already renders a very low COR, $e_{ze} = 0.066$, in a process that requires a longer time to eject the sphere, $\tau_0 = 5.8$ (the values are obtained from the simulation data of Eq. (10) or calculated by Eq. (13a), with results shown in Fig. 1). For any $\lambda > 1.5$, e_{ze} swiftly approaches zero (see Eq. (13)), while requiring even longer ejection times, τ_0 (according to Eq. (13a)). When any one of the CORs, e_{ep} or e_{ze}, approaches zero, Eq. (20) may well render *negative* values for the *apparent* COR, e. The physical meaning is that the sphere continues its motion after impact in the same direction of its pre-impact approaching velocity. Cases like that cannot be physically precluded, however, they are extreme and extraneous to either model, JGM [9] or Zener [2]. Another aspect to consider is that Zener's analysis is a time-dependent process (via the time integration of Eq. (10), with results shown in Fig. 1), while JGM's

analysis is time-independent where the rebound velocity is determined from work-energy principles. It is, therefore, important to recognize that for Eq. (20) to hold, the underlying physical processes of both models must occur concurrently. Said conditions or oddities ought to be monitored and reconciled as necessary.

In the following sections the predictions of the apparent CORs as calculated by Eq. (20) are compared against CORs reduced from experiments [10, 12], and those calculated by full featured FEA simulations [11]. These works by Higgs et al. are chosen because they provide a meticulous description of the diagnostics system (specifically, the high speed camera, as discussed previously), along with all the necessary data to execute Eq. (20) with ease.

Before going to the comparisons, it is important to discuss a few findings by Higgs et al. First they conclude that Zener's CORs do not match the experimental results at all (as their Fig. 6 in [11] shows vast deviations). The same is reported in Ref. [10] (see Fig. 5 there). Based on the discussion above, without the accounting of elastoplastic deformation in the impact, such deviations are not surprising. Also of

Table 2 Material properties for the target plates used in the experiment of [10]

Plate material	Yield strength S_y (Pa)	Density ρ (kg/m^3)	Poisson's ratio ν
Borosilicate glass[b]	1.00E + 12*	2214	0.30
NiTiNOL 60[c]	1.00E + 12*	6700	0.34
S7 Tool Steel[b]	5.52E + 08	7760	0.30
Stainless Steel 440C[b]	4.48E + 08	7750	0.30

Same footnote as for Table 1

Fig. 4 The calculated CORs using Eq. (20) herein for four cases listed in Table 3 given in Ref. [12]. Same symbol shapes represent a given case in Table 3; smaller symbols are the outcome of d = 4.76 mm; larger symbols are the outcome of d = 6.35 mm
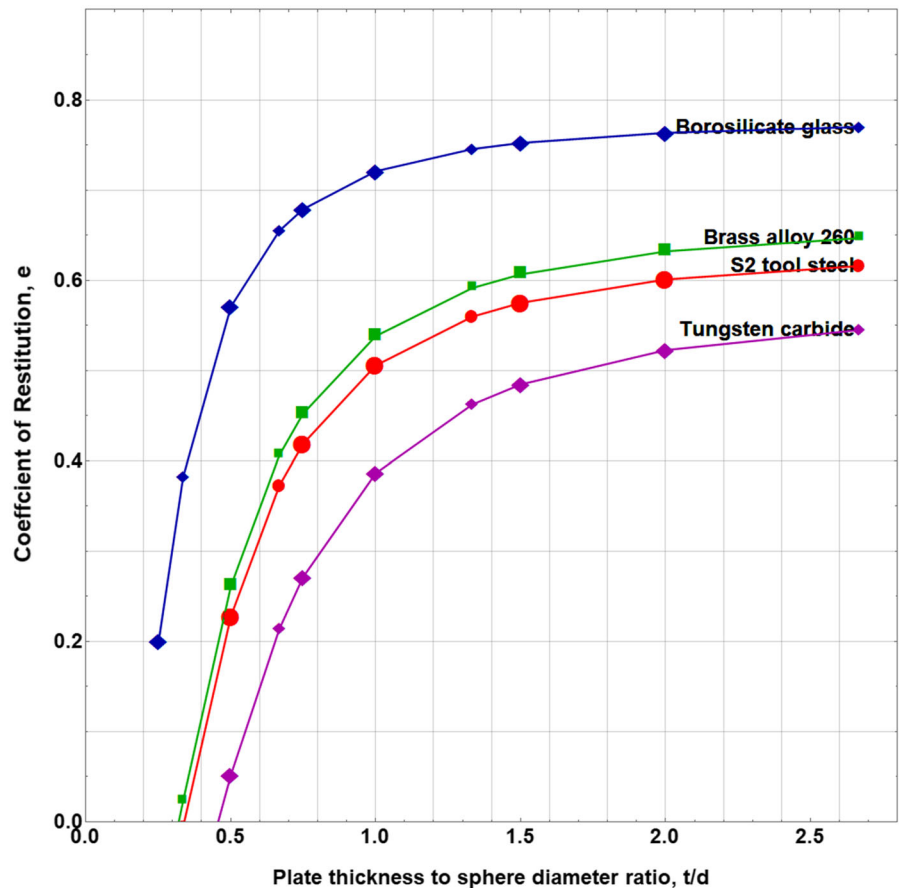
note, is that in Fig. 6 of Ref. [11], the couple of experimentally obtained CORs agree rather well with the predictions given by the JGM model [9], which are recast herein by Eqs. (7) and (8) even though the plate thickness-to-sphere diameter ratios (as seen in Ref. [11]) are about 0.8, and 1.0, i.e., being far from a ratio approaching infinity that represents a half-space. It shall be seen in the coming sections that the fusion of the two models by Zener [2] and by JGM [9] together

into a single expression, Eq. (20), shall provide a remarkable agreement with the CORs given in the three works by Higgs et al. [10–12].

5 Comparison with experimental results

The data for the spheres, plates, and impact velocities are verbatim taken from the work by Marinack et al.

Table 3 Material properties from [12]

Material	Geometry	Elastic modulus (GPa)	Poisson's ratio	Yield strength (GPa)	Density (kg/mm^3)
Brass alloy 260	Sphere	103	0.35	0.393[a]	8525
Aluminum 1100-H16	Sphere	70	0.33	0.103	2710
Tungsten carbide	Sphere	621	0.18	1.720[a]	14,950
S2 tool steel	Sphere	207	0.30	2.00a	7861
Low carbon steel	Sphere	200	0.30	0.303[a]	7833
Borosilicate glass	Sphere	63	0.20	N/A	2214
Aluminum 6061	Plate	69	0.33	0.290	2700

[a]signifies a hardened material

[10]. Tables 1 and 2 provide the material properties for the spheres and plates along with the combinations that have been used. Note that for case numbers 3, 5, and 13 (designated by the added symbol, $) both the spheres and the plates are brittle. For brittle materials ostensibly (extremely) high values of "yield strengths" are assigned to preclude yielding in the calculations, effectively enforcing $e_{ep} = 1$. The results for these cases will be shown separately from the other cases comprising of at least one ductile material. While all the information to execute Eq. (20) is provided in [10], unfortunately the final values for the CORs are not given. Hence, these values had to be extracted by visual inspection from Figs. 3 and 4 in Ref. [10]. Understandably, some inaccuracies might have occurred in that process. The apparent CORs for all cases in Table 1 are calculated by Eq. (20) using $e_{ep} = e_{45}$ (given by Eq. (8)), and the comparison is shown in Fig. 3. The same shape markers and colors belong to the same case, where the open markers are connected by lines to indicate the calculated predicted values by Eq. (20). In some cases, the agreements are just excellent, where in other cases the absolute errors range between 4.5–5.6% with a mean of 5.2%, and the standard deviation ranges between 6.7–7.5% with a mean of 7.2%. In Fig. 3(d) it is obvious that for purely brittle impacts (i.e., purely elastic impacts) the CORs are by and large close to unity, as expected. For such impacts, $e_{ep} = 1$, and Zener's COR predictions are sufficiently accurate. In all cases the CORs decrease with the impact velocities as is predicted by JGM [9], in a tendency that is further explored herein in Section 7. Using $e_{ep} = e_{44}$ instead of e_{45} produces smaller values for the CORs than e_{45}, adding about another 5% to the errors. For the rest of this work e_{45} is used.

More experimental results are given by Patil and Higgs in [12]. That work compares the experimental results given in their Fig. 14, with FEA simulations of [11] (which is discussed in detail in the next section). Table 3 is taken verbatim from Ref. [12]. Experiments were performed with two sizes of sphere diameters $d = \{4.76, 6.35\}$mm. The plates are squared-shape with sides of *152.4 mm*, made of aluminum 6061, but having varying thickness values, $t = \{1.6, 3.18, 4.76, 6.35, 9.53, 12.7\}$mm. The sphere impact velocity is reported to be 2.3 m/s for all cases. For clarity, Patil and Higgs [12] left out the results of the aluminum and low carbon steel spheres; hence, these are not shown here either. The results from using Eq. (20) are shown in Fig. 4. A symbol of the same shape represents a specific material case in Table 3, where the smaller symbols belong to *d = 4.76* mm, and the larger symbols belong to *d* = 6.35 mm. Clearly the symbols for the same material case (i.e., symbols of the same shape) trend together as they represent a certain case in Table 3, specifically at the said impact velocity. Actually, these symbols trend continuously (i.e., on lines) as functions of ratio of *t/d,* which can accommodate any combination of *t* and *d*. Impact velocities higher, or lower than the said 2.3 m/s, would lower, or elevate the lines in the plot, respectively. (This is discussed in a subsequent Section 7.) The most profound finding in Fig. 4 is that now the apparent COR as predicted by Eq. (20) is varying with the ratio of plate thickness to sphere diameter. Such a behavior is lacking from the JGM model [9] (i.e., from either Eqs. (7) and (8)), but now that behavior is inherited from the Zener model [2] (via Eqs. (12) and (13)). Again, the numerical values for the CORs are not given in [12] but close inspection of Fig. 4 herein, and Fig. 14 in [12], reveals not only the same trends, but

Table 4 Material combinations for the FEA simulation cases in [11]

Case	Sphere density ρ (kg/m^3)	Sphere elastic modulus, E (Gpa)	Plate density ρ (kg/m^3)	Sphere elastic Modulus (Gpa)	Plate yield strength, S_y (Mpa)
A1	15,000	800	2000	10	10
A2	15,000	800	2000	10	100
A3	15,000	800	2000	10	1000
A4	15,000	800	2000	10	10,000
B1	2000	10	15,000	800	10
B2	2000	10	15,000	800	100
B3	2000	10	15,000	800	1000
B4	2000	10	15,000	800	10,000
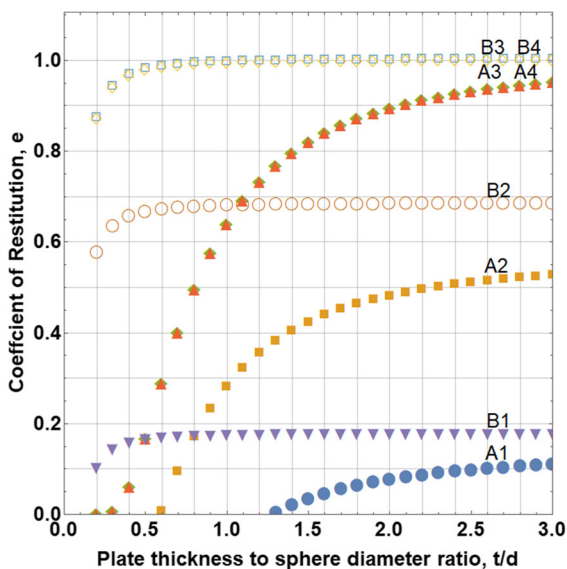
Fig. 5 Calculation of the CORs using Eq. (20) herein for the cases in Table 4 taken from Ref. [11]

more importantly shows that they are very close (if not indistinguishable) in their numerical values. For Borosilicate glass case in particular, but also for the other cases, the results in Fig. 4 herein match better the experimental results in [12] than their own simulation results for *t/d > 1*. Another important observation is that the CORs approach asymptotic values as *t/d* increases. That is because at large enough *t/d* values, Zener's CORs approach unity, and the apparent CORs as seen from Eq. (20) asymptotically approach the values predicted entirely by the JGM [9] model (that corroborates the discussion following Eq. (20) above). That asymptotic trend is visible at *t/d* ratios that are not necessarily "infinitely" large, seemingly that happens

anywhere in the range between *t/d = 1 to 3* depending on the specific parameters of an impact case.

6 Comparison with FEA simulation results

The last comparison of the CORs predicted by Eq. (20) is done against full-scale FEA simulations as detailed in [11]. In that work a parametric FEA study is done on nonreal materials to mimic very wide (and even extreme) ranges of material properties as possible pairs for the impacting sphere and the plate. The material combinations are given in Table 4.

For all materials in Table 4 the Poisson ratio is taken as *0.3,* all are assumed ductile, and for all cases the impacting velocity is 5 m/s. As detailed in the said reference [11], it is noted that the sphere with highest value of density and elastic modulus, and the plate with the lowest value of density and elastic modulus, represent one of the extreme cases for the sphere–plate impact scenarios, which are cases A (i.e., cases A1-A4). And vice versa is the other extreme in cases B (i.e., cases B1-B4).

Physically, cases A represent the impact of the heaviest and stiffest sphere on the lightest and most deformable plates, whereas cases B represent the impact of the lightest and most deformable sphere on the heaviest and stiffest plates (see Table 4). For both cases, the plate yield strength values vary from the weakest or "softest" to the strongest or "hardest." In the said simulations [11], the sphere is assumed elastic; herein, however, that assumption is not necessary as all materials are considered to be ductile, capable of yielding and transition to plasticity. That

Fig. 6 The *apparent* CORs using Eq. (20) for three cases listed in Table 3. Same symbol shapes represent a given case in Table 3. Smaller and larger symbols belong to $d = 4.76$ mm, and $d = 6.35$ mm, respectively. Solid lines belong to $v_o = 2.3$ m/s, where dashed line belong to $v_o = 6.9$ m/s. Zener's COR values, e_{ze}, using Eq. (13) are shown by the dotted lines for $v_o = 2.3$ m/s
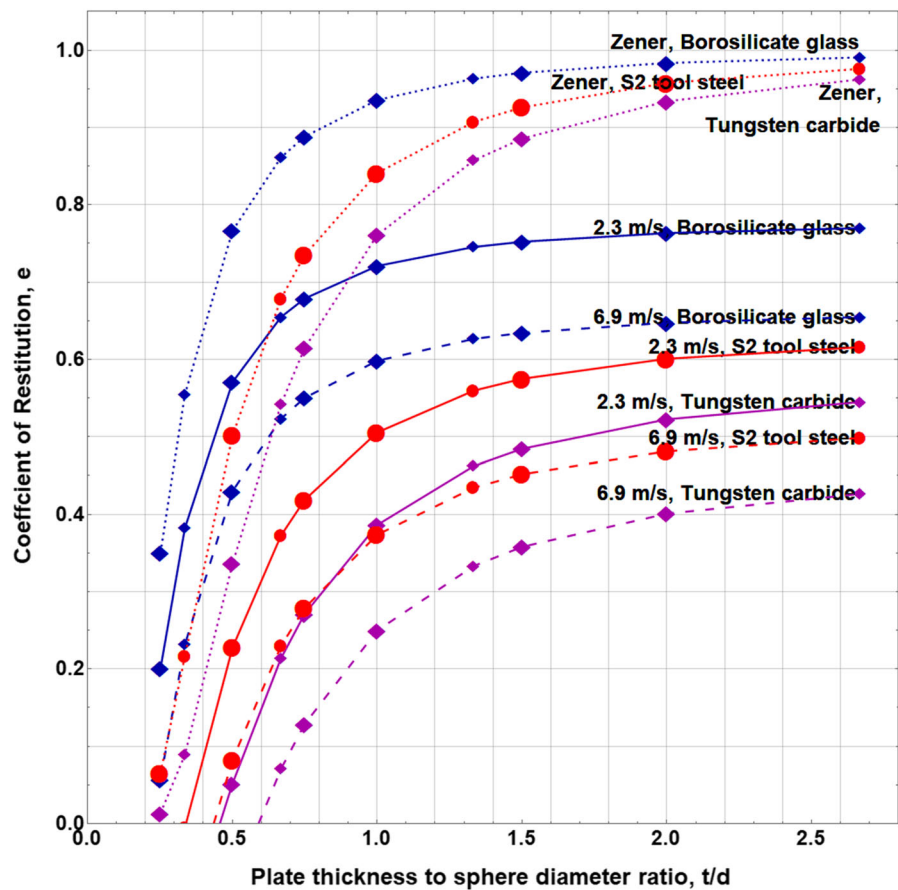
characteristic is straightforwardly accommodated by Eqs. (2) and (3). The results stemming from Eq. (20) are shown in Fig. 5.

Comparing Fig. 5 here with Fig. 7 in Ref. [11] reveals *a remarkable* match for all cases but case A1. Case A1 is an outlier among all cases in Table 4 by having a very "weak" or "soft" plate as it is being impacted by the mostly dense (i.e., "heavy") and "hard" sphere. For all cases A, some λ values equal 1.67 increasing up to 6.68 especially for thin plates (*t/d < 0.5*). These values are outside, and quite far, from Zener's range, $\lambda = \{0, 1.5\}$. Such higher values of λ require much longer contact times τ_0 (see Eq. 13a) while the elastoplastic restitution process might have already completed, ejecting the sphere quite sooner than τ_0. Regardless, all cases asymptotically approach the JGM model [9] as the ratio *t/d* increases (and that behavior has already been discussed above). Because cases A represent impacts of the heaviest and stiffest sphere on the lightest and most deformable plates, the

transition with *t/d* is more gradual then cases B, which represent impacts of the lightest and most deformable sphere on the heaviest and stiffest plates. Hence, for cases B the asymptotic values are reached at much smaller values of *t/d*.

7 The interplay of parameters

Now that Eq. (20) has extensively been verified against experimental and simulation results, it is possible to change parameters to gauge their relative effects upon the COR. For that purpose, the cases in Table 3 are chosen, under the same conditions that produced the results in Fig. 4, only that now Brass alloy 260 is removed for clarity. The first change is that of the impact velocity that is increased threefold. The results are shown in Fig. 6, and as previously, all COR values vary nonlinearly with the ratio, *t/d*. Serving as references for comparison, the solid lines

Fig. 7 The various COR models as functions of the nondimensional impact velocity, V_1^*, for S2 tool steel, and a plate thickness-to-sphere diameter ratio, $t/d = 1$
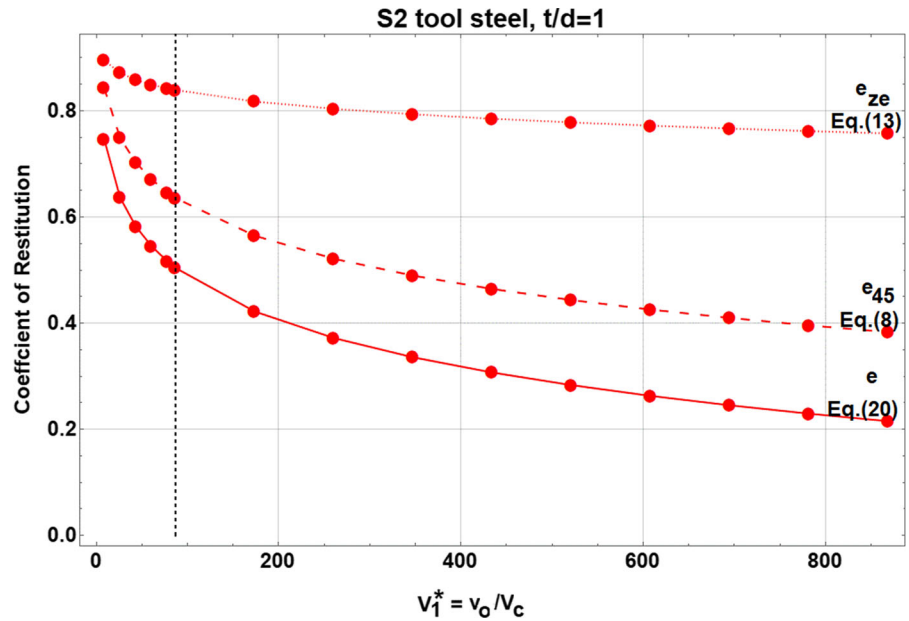
belong to the previous impact velocity of 2.3 m/s, and of course they are identical to those in Fig. 4. The dashed lines correspond to the increased impact speed of 6.9 m/s. It is immediately noticeable that the latter COR values are significantly smaller than the reference benchmarks. The reason is that the added kinetic energy of the sphere, induces additional plastic deformation and damage, causing e_{ep} to decrease (seen by the asymptotic values in Fig. 6). Also, in the Zener model, higher impact velocities, v_o, cause increases in the λ values (see Eq. (12)), resulting in lower values of e_{ze} (see Eq. (13)). Physically, as the deformations of the plate and/or the sphere increase with higher impact velocities, v_o, the elapsed times for the surfaces to recover and rebound are longer, thus causing lower e_{ze} values. The combined drops in both, e_{ep} and e_{ze}, lead yet to smaller values of the overall *apparent* CORs, e, as calculated by Eq. (20).

The second comparison revealed in Fig. 6 is for the pure Zener model of Eq. (13), e_{ze}, at the impact velocity of 2.3 m/s, without any consideration given to elastoplastic deformation or permanent set. The results are depicted by the dotted lines in Fig. 6. Clearly, Zener's model cannot solely represent the *apparent* COR values in collisions of ductile materials. Note also that at the ratio of about $t/d = 1$, Zener's COR values, e_{ze}, are about *0.8* or above, and the *apparent* COR values, as calculated by Eq. (20), continue the increase with t/d but more gradually. At about $t/d = 2$,

$e_{ze} \rightarrow 1$, and the *apparent* CORs have nearly completed the asymptotic approach to the values predicted by JGM [9] (as discussed previously). Definitely, the ratio of $t/d = 2$ is far from representing a half-space. Yet, the COR values predicted by JGM [9], which are based upon a half-space model, are nevertheless borne out. That is not surprising as an impact between a sphere and a plate is a highly localized contact phenomenon. Evidence of such localization can also be found elsewhere, e.g., [18] and [19]. In conclusion, Zener's model comes into play at $t/d < 2$, instigating more profound effects as t/d decreases. For the cases studied, the COR values predicted by JGM [9] are sufficiently accurate for $t/d > 2$.

To gauge the effects of impact velocities while holding all of the other parameters constant, the case of S2 tool steel (being at an intermediate range of COR values in Fig. 4) is selected for further investigation while purposely holding $t/d = 1$. The impact velocity is now varied from 0.1 to 10 times the velocity of 2.3 m/s (the one used previously for the analysis of Fig. 4). The critical velocity calculated by Eq. (5) is $V_c = 0.0265 \ m/s$. Figure 7 shows the three COR models, as functions of the normalized impact velocity, $V_1^* = v_o/V_c$. The effects of Zener's Eq. (13), and JGM's Eq. (8) are shown separately from each other by the dotted and dashed lines, respectively. Then they are combined together into the current new model given by Eq. (20), and shown in Fig. 7 as well by the

solid line. The nondimensional impact velocity case that is specifically relevant to Figs. 4 and 7 is $V_1^* = 2.3/V_c = 86.9$, which is identified by the vertical dashed line at that specific nondimensional velocity value. The nonlinear decreases in e_{ze}, and e_{45} with the increase of the impact velocity is moderate according to Eq. (13), but steeper according to Eq. (8), respectively, which is expected for ductile materials. Indeed, the previous discussion on the changes in the kinetic energy (portions of which are absorbed in the collision) is reinforced by the trends shown in Fig. 7. Specifically, at $V_1^* < 86.9$ the CORs are larger than the reference case in Fig. 4, and at $V_1^* > 86.9$ the CORs are smaller. Note that the COR values in Fig. 3 also decrease with the impact velocity, albeit the velocity range there is quite small.

8 Conclusions

In this work an analytical expression to determine the *apparent* COR is sought to fuse two existing models where each separately accounts for different effects. The earliest of the two models is that by Zener who presented a theory of a sphere pinging a thin plate in a purely elastic contact using the classical Hertz solution. An empirical, yet an accurate fit is provided herein for Zener's COR values. These stem from the numerical integration results of Zener's nonlinear ODE. A mechanical equivalent is envisioned to mimic the impact problem between a sphere and a plate. That mechanical equivalent is fused with an available model by JGM, which accounts for elastoplastic deformation that is expected to occur in ductile materials. The fused model is *extensively* verified against data stemming from laboriously obtained experimental results and FEA simulations. Overall, the agreement for all cases is very good to spot-on, with perhaps the exception of a couple of extreme cases that show some discrepancies (as monitored and analyzed herein). Those cases are most likely to disobey certain assumptions of either or both of the two models that comprise the analytical expression for the *apparent* COR. Besides knowing the material properties and geometries of the impacting bodies, all that is needed is the sphere impacting velocity, and the *apparent* COR is readily calculated by Eq. (20).

Declarations

Appendix

The Expanded Form of Eq. (10), its Linearization and Limits

The expanded form of Eq. (10) is simply:

$$\frac{d^2\sigma}{d\tau^2} + \frac{3}{2}\lambda\sqrt{\sigma}\frac{d\sigma}{d\tau} + \sigma^{\frac{3}{2}} = 0 \tag{21}$$

This equation is nonlinear because of Zener's selection of the Hertzian contact model. Indeed, that model is suitable for the contact between a solid sphere and a half-space, featuring a nonlinear force–displacement relationship, $F(s) = ks^{3/2}$. That produces nonlinear exponents for σ in Eq. (21). It is immediately apparent that Eq. (21) would render a complex solution if σ is allowed to become negative. A complex solution, however, is not physical for the real problem at hand. Further discussion is offered below.

Suppose that a linear force–displacement relationship existed instead, where $F(s) = ks$. Applications having such a relationship are: (i) impact (i.e., contact) between a cylinder on its flat end, and an elastic half-space, for which $k = 2RE'$, and (ii) impact between a cylinder along its length, L, with an elastic half-space that has $k = \pi LE'/4$. The parameter λ may also differ from Zener's definitions, but regardless of the application, σ would still be raised to the first power, and Eq. (10) would become:

$$\frac{d^2\sigma}{d\tau^2} + \lambda\frac{d\sigma}{d\tau} + \sigma = 0 \tag{22}$$

Fig. 8 Zener's COR results as functions of the parameter λ, for the nonlinear Eq. (10), shown in solid blue, and the linearized Eq. (22), shown in solid red. Curve fits for both Eqs. (13) and (23) are, respectively, shown by the dashed lines. The inset shows the same in semi-log scale
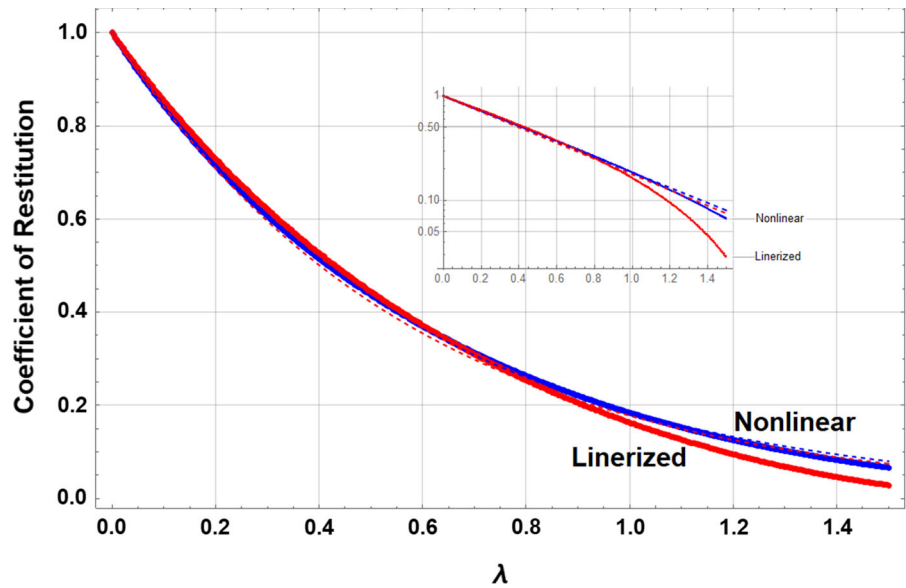
This linear equation is fundamental in vibrations theory, representing a homogeneous equation of motion for a single degree of freedom system consisting of a mass, a spring, and a damper (as seen in Fig. 2(b)-the damper, though, is not shown). Seemingly, λ takes on the role of the damping coefficient. Hence, Eq. (22) signifies a linearized version of Eqs. (10), or (21). While Eq. (22) does render real solutions even for $\sigma < 0$, those are meaningless as they are still not physical (discussed further below).

The analytical solution to Eq. (22) is well known, and the extraction of the COR from that solution could be obtained analytically. Alternatively, there is an effortless way to achieve that. The same procedure (i.e., computer code) that resulted in Eq. (13) is now tasked with Eq. (22) as the objective (instead of the previously used Eqs. (10), or (21)). The results are shown in Fig. 8. The CORs as functions of λ are shown for two cases: (i) from the solution of the original nonlinear Eq. (10), and (ii) from the solution of the linearized Eq. (22). The CORs resulting from the two solutions are nearly inseparable up to about $\lambda = 1$. A similar curve-fit procedure is performed here for the latter case as well, resulting in:

$$(e_{ze})_{linear} = \exp(-1.72847\lambda) \tag{23}$$

Both Eqs. (13) and (23) are also shown by dashed lines in Fig. 8, and by observation they can barely be distinguished from each other, and from the data up to about $\lambda = 1$. The immediate conclusion is that Zener's predicted CORs are quite insensitive to the selection of the contact model. It is also clear now that Eq. (14) is only a special case of Eq. (22), and that in fact the latter can replace the former for other values of λ. This further supports the use of the mechanical equivalent of Fig. 2(b) for a range of λ, certainly up to $\lambda = 1$. A universal expression of $e_{ze} = \exp(-1.7\lambda)$ may collectively be used with sufficient accuracy to represent Zener's CORs, regardless of the contact model employed.

An important qualification (restriction) must be recognized in regards to the force–displacement relationship, whether it is nonlinear, $F(s) = ks^{3/2}$, or linear, $F(s) = ks$. Zener's model of Eqs. (10), or (21), and the linearized version of Eq. (22), are valid *if and only if* the interference, s, is nonnegative so that $F(s)$ is a compressive contact force. Once $s = 0$ (or $\sigma = 0$) emerges on the rebound signifying ejection onset, contact is lost, $F(s) = 0$, and that occurs at the nondimensional instant of $\tau \equiv \tau_0$ (see Eqs. (13), and the pertinent discussion there). Equations (10), (21), and (22), are irrelevant past any $\tau > \tau_0$, as the impacting body (e.g., a sphere) is no longer in contact with the plate, and it would be governed by different kinetics after the rebound. Problems of reoccurring impact, intermittent contact, and rubbing dynamics are commonly handled by a Heaviside function or other contact models as applied in [20–24]. In the

framework of a single impact, undergoing only compressive phases of deformation and restitution, $F(s) \geq 0$, and $\tau \leq \tau_o$. These set validity limits on Eqs. (10), (21), and (22), which ought to be recognized.

References

1. Meriam, J.L., Kraige, L.G., Bolton, J.N.: Engineering Mechanics: Dynamics. John Wiley & Sons (2020)
2. Zener, C.: The intrinsic inelasticity of large plates. Phys. Rev. **59**(8), 669–673 (1941)
3. Raman, C.V.: On some applications of hertz's theory of impact. Phys. Rev. **15**(4), 277–284 (1920)
4. Tsai, P.-K., Li, C.-H., Lai, C.-C., Huang, K.-J., Cheng, C.-W.: Approximation solution for the zener impact theory. Mathematics **9**(18), 2222 (2021)
5. Zhu, R., Liu, X.N., Huang, G.L.: Study of anomalous wave propagation and reflection in semi-infinite elastic metamaterials. Wave Motion **55**, 73–83 (2015)
6. Khan, M.H., Li, B., Tan, K.T.: Impact load wave transmission in elastic metamaterials. Int. J. Impact Eng **118**, 50–59 (2018)
7. Wen, K., Chen, X.: Analysis of the stress wave and rarefaction wave produced by hypervelocity impact of sphere onto thin plate. Defence Technol. **16**(5), 969–979 (2020)
8. Moon, S.-I., Kang, T., Seo, J.-S., Lee, J.-H., Han, S.-W., Park, J.-H.: Plate bending wave propagation behavior under metal sphere impact loading. J Mech Sci Technol **32**(3), 1117–1124 (2018)
9. Jackson, R.L., Green, I., Marghitu, D.B.: Predicting the coefficient of restitution of impacting elastic-perfectly plastic spheres. Nonlinear Dyn **60**(3), 217–229 (2010)
10. Marinack, M.C., Musgrave, R.E., Higgs, C.F.: Experimental investigations on the coefficient of restitution of single particles. Tribol. Trans. **56**(4), 572–580 (2013)
11. Patil, D., Fred Higgs, I.C.: Critical plate thickness for energy dissipation during sphere-plate elastoplastic impact involving flexural vibrations. J. Tribol. **139**(4), 041104 (2017)
12. Patil, D., Fred Higgs, C.: Experimental investigations on the coefficient of restitution for sphere-thin plate elastoplastic impact. J. Tribol. **140**(1), 011406 (2018)
13. Banerjee, A., Chanda, A., Das, R.: Historical origin and recent development on normal directional impact models for rigid body contact simulation: a critical review. Arch. Comput. Meth. Eng **24**(2), 397–422 (2017)
14. Jackson, R.L., Green, I.: A finite element study of elastoplastic hemispherical contact against a rigid flat. J. Tribol. **127**(2), 343–354 (2005)
15. Etsion, I., Kligerman, Y., Kadin, Y.: Unloading of an elastic-plastic loaded spherical contact. Int. J. Solids Struct. **42**(13), 3716–3729 (2005)
16. Jackson, R., Chusoipin, I., Green, I.: A finite element study of the residual stress and deformation in hemispherical contacts. Trans. ASME-F-J. Tribol. **127**(3), 484–493 (2005)
17. Green, I.: Poisson ratio effects and critical valus in spherical and cylindrical hertzian contacts. Appl. Mech. Eng. **10**(3), 451 (2005)
18. Yang, H., Green, I.: An elastoplastic finite element study of displacement-controlled fretting in a plane-strain cylindrical contact. J. Tribol. **140**(4), 041401 (2018)
19. Yang, H., Green, I.: A fretting finite element investigation of a plane-strain cylindrical contact of inconel 617/incoloy 800h at room and high temperatures. Proc. Instit. Mech. Eng. , Part J: J. Eng. Tribol. **233**(4), 553–569 (2019)
20. Varney, P., Green, I.: Nonlinear phenomena, bifurcations, and routes to chaos in an asymmetrically supported rotor-stator contact system. J. Sound Vib. **336**, 207–226 (2015)
21. Varney, P., Green, I.: Rotordynamic analysis of rotor-stator rub using rough surface contact. J. Vib. Acoust. **138**(2), 021015 (2016)
22. Smyth, P.A., Varney, P.A., Green, I.: A fractional calculus model of viscoelastic stator supports coupled with elastic rotor-stator rub. J. Tribol. **138**(4), 041101 (2016)
23. Varney, P., Green, I.: Rough surface contact of curved conformal surfaces: an application to rotor-stator rub. J. Tribol. **138**(4), 041401 (2016)
24. Varney, P., Green, I.: Impact phenomena in a noncontacting mechanical face seal. J. Tribol. **139**(2), 022201 (2017)